JOURNAL OF CATALYSIS 73, 91–103 (1982)

UHV Studies of the Interaction of CO with Small Supported Metal Particles, Ni/Mica

D. L. DOERING, J. T. DICKINSON,[1] AND H. POPPA[2]

Stanford/NASA-Ames Joint Institute for Surface and Microstructure Research, NASA, Ames Research Center, Moffett Field, California 94035

Received May 5, 1981; revised September 21, 1981

The interaction of carbon monoxide with small nickel (Ni) particles supported on UHV-cleaved mica was studied using flash thermal desorption, Auger electron spectroscopy, and transmission electron microscopy. Molecular desorption was accompanied by decomposition of CO at a rate strongly dependent on particle size. Recombination of surface-precipitated carbon with adsorbed oxygen was observed, and gas-induced morphological particle changes because of exposure to CO and O_2 are analyzed in some detail.

INTRODUCTION

One of the key steps in a number of catalytic reactions, such as the carbon monoxide methanation reaction on nickel (Ni), is the dissociation of CO (*1–3*). Ultra high-vacuum (UHV) studies on low-index planes of single-crystal Ni have shown that CO dissociation typically occurs at temperatures above that of the CO desorption peak (*4–6*). The activation energy for CO decomposition was found to be lowered on Ni surfaces that have structural damage, e.g., grain boundaries, steps, or sputtering defects (*7–9*). This could be important for various catalytic processes.

Particulate Ni films might be expected to behave similar to a stepped or damaged surface with regard to the activity toward CO decomposition. This should be particularly true for very small particles because of the high density of edge and corner sites.

In this study, the interaction of CO and O_2 with particulate Ni films is investigated by a combination of flash thermal desorption (FTD), Auger electron spectroscopy (AES), and transmission electron microscopy (TEM). Results show that, (1) CO decomposes on Ni clusters at a rate strongly dependent on particle size, especially for clusters below 5 nm in diameter, (2) the associative desorption of carbon with adsorbed oxygen varies in temperature with the oxygen coverage, and (3) exposure to gas and thermal treatments causes morphological particle changes.

EXPERIMENTAL

For model studies of gas interactions with well-defined supported metal particles, a UHV system of two chambers was constructed; a sample preparation chamber and a smaller-volume reaction chamber (see Fig. 1). The chambers were separately pumped and could be isolated from one another during dosing and desorption/reaction experiments. This eliminated reactions from undefined surfaces in the preparation area. The reaction chamber was pumped with a closed-cycle He cryopump with a very high pumping speed, producing essentially no backstreaming of impurity gases during dosing. The preparation chamber was ion pumped. Both chambers routinely reached base pressures below 2×10^{-10} Torr (1 Torr = 133 N m^{-2}).

High-grade natural mica (muscovite) was used as a substrate material. Mica is an

[1] Permanent address: Physics Department, Washington State University, Pullman, Wash. 99164.

[2] To whom correspondence should be addressed.

0021-9517/82/010091-13$02.00/0

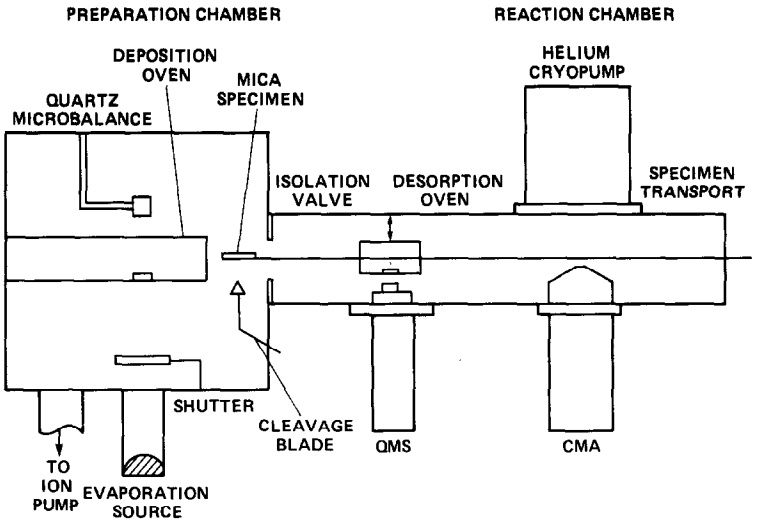

FIG. 1. Schematic diagram of the experimental system.

excellent support material for several reasons. First, the gases of interest in these experiments (CO, CO_2, and O_2) do not adsorb on mica. Second, particle growth of several metals has been studied on mica (*10–12*). Third, clean surfaces are easily obtained by cleaving the sample under vacuum. [Auger analysis of a freshly cleaved sample reveals only oxygen, potassium, silicon, aluminum, and traces of iron which are all typical (*13*).] Finally, specimens are easily prepared for subsequent TEM analysis by the mica stripping method described in detail by Lee (*14*), except that an evaporated carbon layer was not deposited on the samples before stripping.

Although samples were exposed to atmosphere during the preparation and transfer process for TEM, substantial changes in the particles are not believed to occur. Untested Ni deposits were observed by transmission electron diffraction (TED) to have not been oxidized by air exposure. Also, changes in the particles due to relatively minor *in situ* gas–thermal treatments (to be mentioned under Results) were still observable by TEM. (A preliminary *in situ* TEM study involving air exposure of small Pd particles (as small as 1 nm) on recrystallized alumina films showed no observable change either.)

Untreated mica has a fairly high concentration of water incorporated into its bulk. The concentration of water on the surface plays an important role in metal particle nucleation and growth (*15*). To achieve reproducible surface conditions for metal deposition, the mica was heated for 24 hr at 450°C. Then, each metal deposition was preceded by cleaving of the mica and annealing for 15 min at 450°C.

Vapor deposition by electron beam evaporation of a high-purity Ni source produced the particulate films on the mica. The size, morphology, and orientation of the particles are controlled by the substrate temperature, metal flux, and the deposition time. A constant substrate temperature of 300°C during deposition was achieved by surrounding the sample with a cylindrical oven. A rectangular aperture in the oven wall defined the area of the deposit which was about 0.3 cm^2. A quartz crystal microbalance was used to monitor the metal flux to the sample which was held at 2.9×10^{14} atoms/cm^2/sec for all samples. The deposition time was controlled by a manually operated shutter between the metal source and the mica. Deposition times ranged from 1 to 200 sec for samples in this study.

The background gas pressure in the system during metal deposition was typically

about 3×10^{-9} Torr. The primary gases were found to be CO, CO_2, H_2, and H_2O. At this low pressure and with elevated substrate temperatures for the deposits, no effects of the residual gases on the metal films and their structure were noticed.

After deposition, the sample was returned to the reaction chamber which was equipped with a quadrupole mass spectrometer (QMS), an Auger electron spectrometer, and an oven for sample desorption heating. CO, O_2, and H_2 gases could be leaked into the system for adsorption–desorption or reaction studies by mechanical UHV leak valves. During CO or H_2 dosing, background impurities remained below 1% of the signal as measured by the QMS. Oxygen exposures were usually accompanied by increases in the H_2O, CO, and CO_2 signals due to replacement reactions within the system. These gases accounted for less than 6% of the total pressure and could be easily differentiated from the reaction products of the sample. Following the closure of the leak valves, the normal background pressure was restored within seconds due to the high pumping speed of the cryopump.

Thermal desorption spectra were obtained by rapidly inserting the specimen into the desorption oven and then measuring the product gases as a function of time with the line-of-sight QMS. The preset temperature of the desorption oven determined the heating rate of the sample. The surface temperature (T) vs time (t) could not be determined directly. However, it could be approximated from temperature calibrations obtained for a continuous metal film by attaching a thermocouple to the mica with silver paste as reported previously (*16*). This yielded the function: $T = (T_f - T_0)[1 - \exp(-\alpha t)] + T_0$, where T_f is the maximum temperature of the sample in the oven, T_0 is the initial sample temperature, and α is a constant which is dependent on the oven temperature. This temperature function is, of course, only an approximation for particulate deposits because exposed mica is a better absorber of infrared radiation than metals. Thus, the quoted temperatures are considered to be low. However, comparisons of desorption spectrum features should be reliable because, (1) reproducibility for samples prepared and tested under identical conditions was excellent, and (2) the variation in actual heating rate should be quite small over the relatively narrow range of metal coverages used in most of this study. The oven temperature was held at 350°C for all CO desorptions and at 450°C for C–O recombination tests. Desorption spectra are shown as a function of time rather than of temperature, but desorption features will be characterized by temperatures approximated from the calibration mentioned above.

AES provided a measure of the amount of metal deposited on the mica surface. For very small particles (under 2 nm diameter), practically all of the metal atoms are at the surface and therefore contribute to the AES signal. However, with larger particles, attentuation of the Auger electrons from deeper metal atoms must be considered. Nevertheless, in the range of deposit thickness used, the Auger signal for "as-deposited" samples can still be used as a monitor of the amount of metal on the mica surface. In addition, AES was used to detect changes in the dispersion of the metal deposits (for particles larger than twice the escape depth of the Auger electrons) assuming that not metal atoms are lost from the surface during our gas–thermal treatments. Thus, coalescence of the particles would cause some attenuation of the Auger signal. Likewise, any redispersion of the particles should be accompanied by either no change in the signal (if the particles are initially very small) or an increase in the signal. Finally, AES provides a means for the detection of contamination on the sample. Because of the number of Auger peaks from the mica constituents and from the metal deposit, it is difficult to detect some contaminants. However, carbon contamination was followed closely during CO adsorption–desorption cycles.

Electron beam irradiation is known to

decompose the mica surface (*13*). Also, electron beam exposure is known to decompose CO on Ni (*5*). Therefore, the electron beam current density and the exposure of the sample to the beam were held to the minimum levels with acceptable signal–noise during AES; whenever possible, Auger measurements were performed without adsorbed gases on the Ni particles.

RESULTS

1. Sample Characterization

Samples with various Ni exposures were removed from the system "as deposited" and analyzed by TEM/TED. The average particle diameters and number densities of these samples are shown as a function of deposition time in Fig. 2. Ni exposures of 5 to 50 sec produced particles with average sizes which increased almost linearly with time from 1.6 to 5.4 nm. Examples of these deposits are shown in Fig. 3. The particle number density grew rapidly to a peak of about 2.5×10^{12} particles/cm^2 after 15 sec of deposit. The number density was reduced by further deposition due to particle coalescence. The Ni deposits were observed by TED (see Fig. 3) and exhibited only weak textures in contrast to a greater degree of epitaxy expected for higher substrate temperatures (*10*).

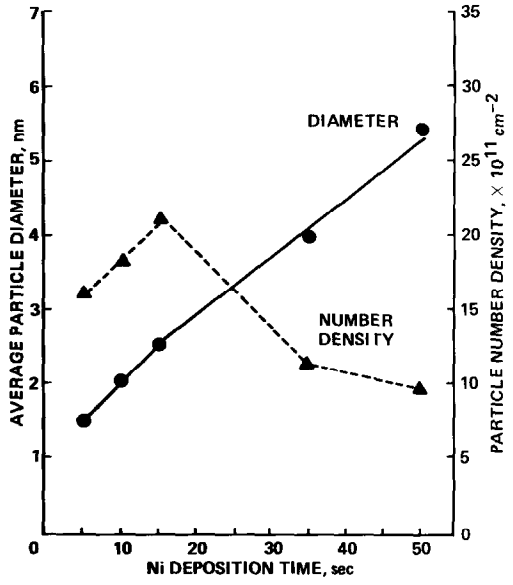

FIG. 2. Average diameter and number density of Ni particle grown on mica vs deposition time. The Ni flux and substrate temperature during deposition were 20 nm/min and 300°C, respectively.

Nickel deposits of longer than 50 sec produced particle size distributions with two distinct maxima due to secondary nucleation of particles. Most of the chemisorption results we present are limited to samples with shorter deposition times and correspondingly simple size distributions.

Because of the difficulties encountered with the TEM detection of very small metal particles, the average particle size of the smallest deposits used in this study is most likely overestimated. A Ni deposit of only 1.5 sec produced an easily detectable CO desorption signal, but no particles could be positively identified by standard TEM. By extrapolation of the particle diameter curve identified by standard TEM. By extrapolation of the particle diameter curve in Fig. 2 to smaller deposition times, the average particle size of this deposit would be about 1 nm.

The growth of Ni on the mica surface was monitored by AES as a function of metal exposure. The Ni 848-eV Auger peak was used for most of this study because an aluminum Auger transition from the mica interfered with the more surface sensitive 61-eV Ni peak for small deposition times. The Ni 848-eV Auger peak grew linearly with metal exposure up to a deposition time of 20 sec where the particles were around 3 nm in diameter and the growth rate decreased. In Fig. 4, the Ni Auger peak height vs metal exposure is plotted.

Immediately after the Auger spectra were recorded, the samples were exposed to a saturation dose of CO [greater than 6 L (1 L = 10^{-6} Torr sec)] and a FTD was performed. The CO desorption peak areas are also plotted in Fig. 4. (Because of the high pumping speed, the desorption peak area is proportional to the total gas desorbed (*17*).) Assuming an adsorption stoi-

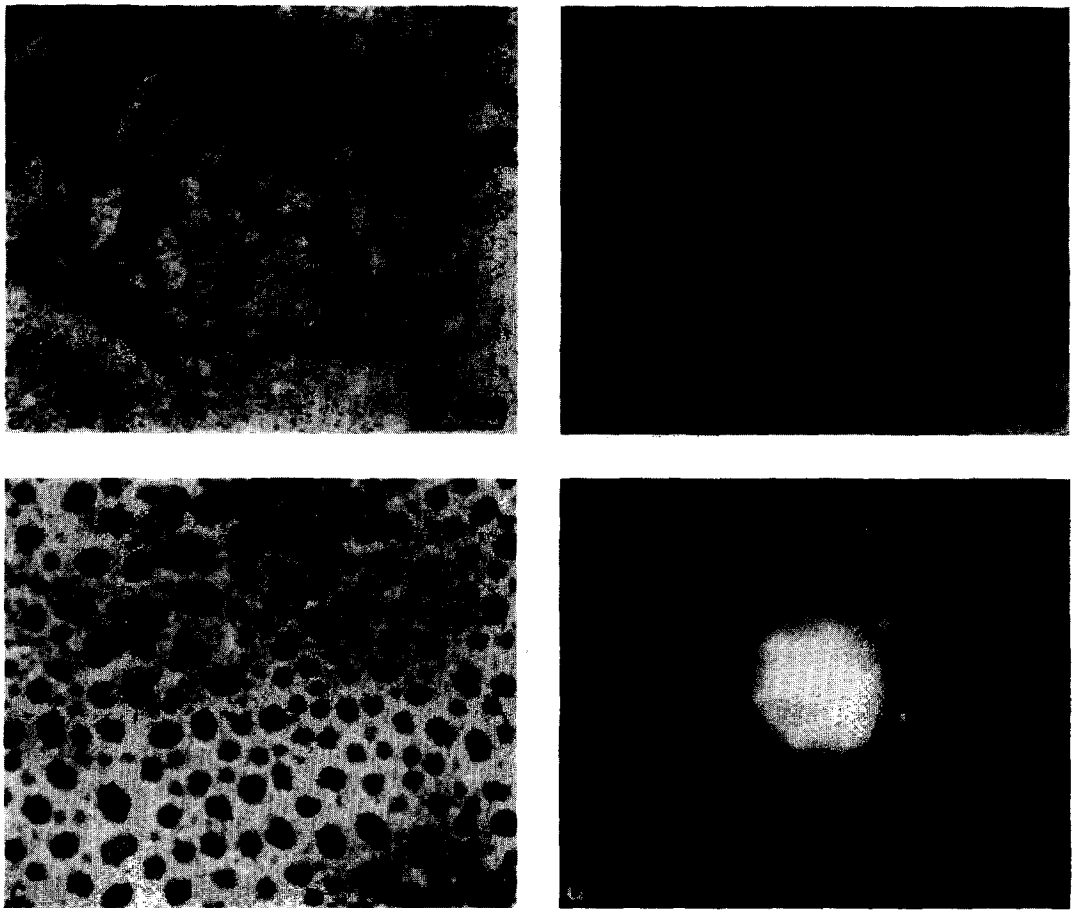

FIG. 3. Representative transmission electron micrographs of Ni particles grown on mica: (a) 5-sec deposition time (1.6 nm average particle size); (b) 25-sec deposition time (33 nm); (c) 50-sec deposition time (5.4 nm); and (d) transmission electron diffraction pattern of the deposit in (c). The metal flux and substrate temperature during deposition were 20 nm/min and 300°C, respectively.

chiometry that is independent of particle size, this area is a direct measure of the surface area of the metal. Initially, the FTD peak area increases linearly with metal exposure; after 10 to 15 sec the slope decreases. The change in slope of both the metal Auger signal and the CO FTD peak area is due to the growth of three-dimensional particles. As the particles grow, an increasing percentage of the metal atoms become "bulk" atoms, which contribute less to the Auger signal (Auger escape depth of the 848-eV electrons is about 1.3 nm) and none to the CO desorption. Therefore, the change in slope of the CO FTD peak area occurs earlier in deposition time than the corresponding change in the Ni AES signal.

2. *Adsorption and Surface Reactions*

Figure 5 shows the first CO desorption spectrum from a set of samples with different metal deposition times ranging from 1.5 to 100 sec. Each spectrum was taken about 15 min after deposition of the metal was complete. The time of the desorption maximum (peak time) was observed to increase with metal exposure. Assuming identical heating rates, which is reasonable for these low metal exposures, the total shift in tem-

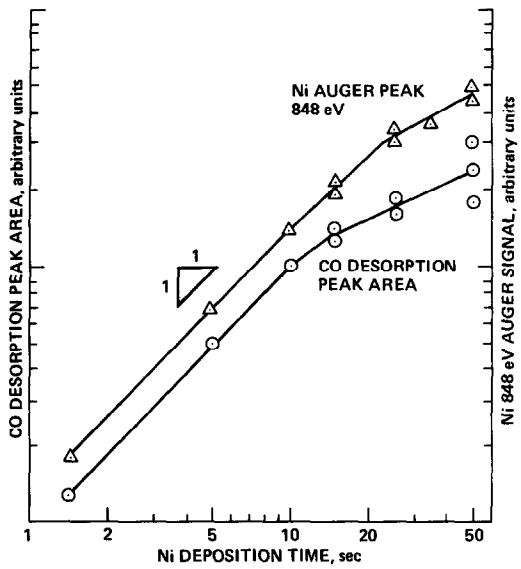

FIG. 4. The peak–peak height of the Ni 848-eV Auger signal and the area under the CO desorption peak vs Ni deposition time plotted on a log–log scale.

perature was about 20°C. For metal exposures greater than 100 sec (not shown), the peak temperature was independent of the metal exposure.

As shown previously for Pd particles on mica (*18*), a steady loss of the CO desorption peak area occurs during successive adsorption–desorption cycles from small Ni particles. Primarily, this loss is from the high-temperature side of the peak causing an apparent shift in the peak to lower temperature. The reduction of the peak area with the number of desorptions was nearly linear initially; after a substantial reduction, further losses appeared exponential with the number of desorptions. (The average reduction in the CO FTD peak area per flash is referred to here as the peak decay rate.) The decay of the CO desorption peak area was accompanied by a corresponding increase in the carbon (C) 272-eV Auger peak (a direct measure for the buildup of C on the particle surface). These effects can be observed for a 15-sec Ni deposit in Fig. 6.

The desorption peak decay rate (in percentage of the original desorption peak area) and the average rate of increase of the C Auger peak per flash (in percentage of the original Ni Auger peak–peak height) are shown as a function of average particle size in Fig. 7. It can be seen that the rate of carbon buildup per flash follows the same behavior as the FTD decay rate. For deposits with particles less than 5 nm in size, the decay rate increases rapidly with diminishing size. For the smallest particles, over 20% of the peak area was lost with each desorption. Thus, the FTD decay is interpreted as being due to an accumulation of surface carbon during the adsorption–desorption cycles.

Surface carbon can also be identified chemically on Ni particles by dosing C-contaminated samples with a small amount of oxygen at room temperature before FTD. A CO desorption peak (β_1) is observed at about 250°C; this is much higher than the standard molecular (α) CO desorption peak at around 130°C. A corresponding reduction of the C Auger peak is observed fol-

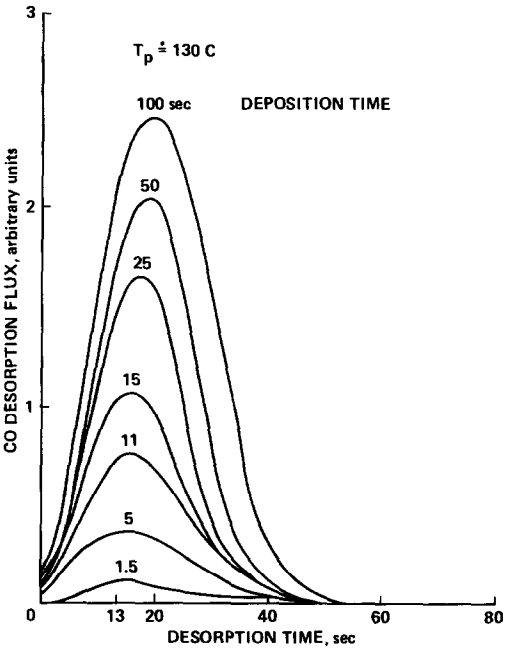

FIG. 5. First CO desorptions from particulate Ni films with various metal exposures. The CO dose for all samples was 6 L (6×10^{-6} Torr × sec).

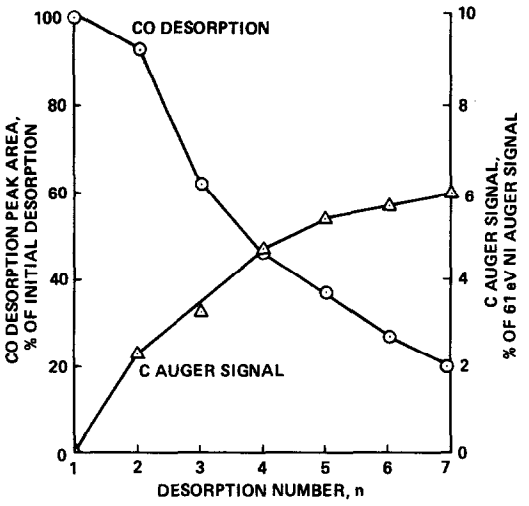

FIG. 6. Carbon 272-eV Auger signal and CO desorption peak area during successive CO desorptions for a 15-sec Ni deposit (6-L CO doses). The C Auger signal was normalized as a percentage of the Ni 61-eV signal.

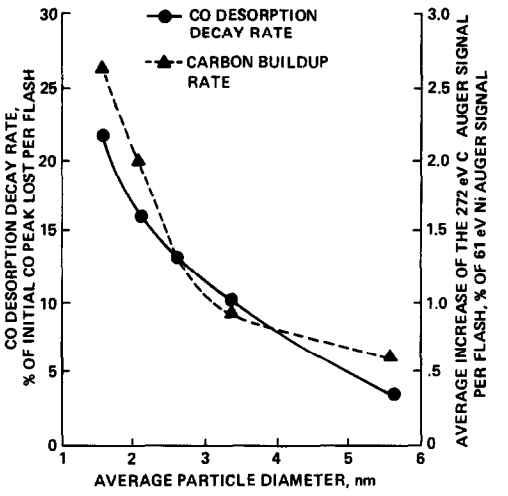

FIG. 7. Carbon deposition rate on Ni particles during successive CO adsorption–desorption cycles vs particle size. Surface carbon was measured by the average change in both the CO desorption peak area and the C 272-eV Auger peak per desorption.

lowing this process. When the oxygen coverage was increased for a given C coverage, the β_1 peak temperature decreased until a minimum was reached. In Fig. 8a, successive flashes of a C-contaminated 25-sec Ni deposit preexposed with 5 L of O_2 are shown. (Notice the higher desorption oven temperature of 450°C.) The β_1 CO desorption peak area was proportional to the C coverage and did not shift in temperature (about 200°C). The appearance of the β_1 desorption peak and the effect of varying the oxygen coverage on CO desorption from Ni have been observed on single-crystal Ni (*6*, *8*); they were attributed to the associative desorption of carbon and oxygen atoms from the Ni surface.

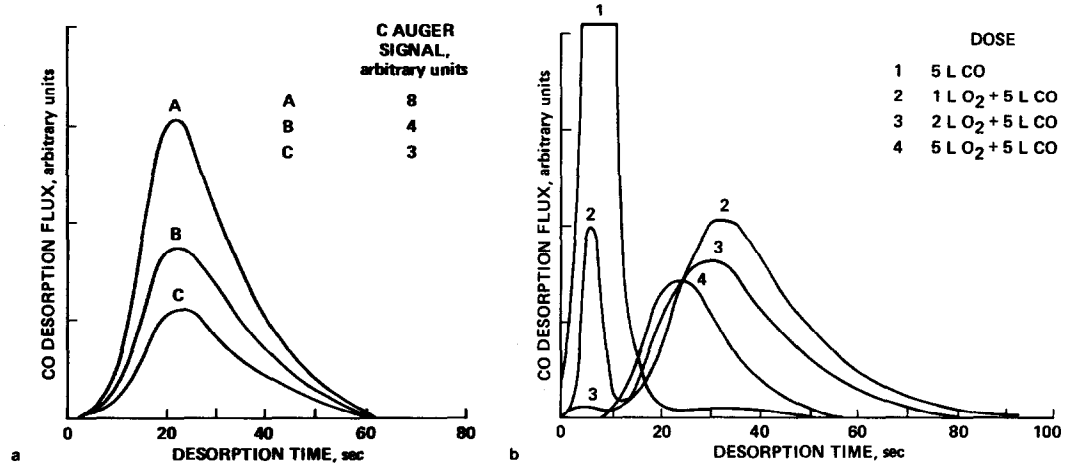

FIG. 8. CO desorption from C-contaminated Ni particles with a 3.3-nm initial average size; (a) exposed to oxygen alone with three different C coverages (5-L oxygen doses), (b) successive desorptions following adsorption of oxygen and CO (oxygen adsorbed first). The oven temperature was 450°C for these desorptions.

When a C-contaminated sample was exposed first to O_2 then to CO, the molecular (α) and the β_1 desorption states were observed [see Fig. 8b]. The α and β_1 peaks both shifted to lower temperatures with increasing O_2 exposure. The shift of the α peak is again consistent with work on single-crystal Ni (*19*). The reduction of the molecular CO binding energy was sufficient to inhibit CO adsorption at the adsorption temperature (50°C) used in our work. Thus, the α peak decreases in amplitude with increasing O_2 exposure.

Extensive heat treatment of the contaminated particles in oxygen, e.g., 10 min at 300°C in 5×10^{-7} Torr of O_2, succeeded in completely removing the carbon. However, residual oxygen strongly inhibited CO adsorption following such a treatment. This oxygen could be removed by heat treatments with H_2. For continuous Ni films (where oxygen on the Ni could be monitored by AES without interference from the mica), surface oxygen was removed by several minutes exposure to 5×10^{-7} Torr of H_2 at 300°C. No effort was made to optimize these cleanup reactions. However, such treatments had a significant effect on particle morphologies and their state of dispersion.

3. Gas-Induced Changes in Particle Morphology

During the first few desorptions of a FTD series, the CO desorption peak from Ni particles moved to higher temperatures; in contrast to Pd, where the peak shifted in the opposite direction (*18*). For the smallest Ni deposits, the upward temperature shift of the peak was quickly overcome by the shift to lower temperature caused by the rapid buildup of surface carbon. However, for midsized particles (2.5 to 5 nm), the peak position approached that of the 100-sec deposit (see Fig. 5). The shift to higher temperature is shown in Fig. 9a for a 25-sec Ni deposit with an average particle size of about 3.5 nm. When a similar sample was subjected to a 5-min vacuum anneal at 300°C immediately after deposition, the first CO FTD peak was unchanged from that of an unannealed sample; further CO desorptions again produced an upward shift in the peak time. Thus, CO induced a change in the Ni particulate deposits which alters the desorption kinetics. Similarly, the variation in peak temperature of the first CO desorption with particle size (see Fig. 5) is interpreted as being due to differences between the morphology of small and large particles.

The first few desorptions also affected the Ni Auger peak amplitude. Initially the Auger peak decreases rapidly, then more slowly with further desorptions. Repeated insertions of samples into the oven without CO preexposure do not change the Ni Auger peak height; subsequent CO desorptions again produce Ni Auger peak reductions [see Fig. 9b for this result on a 15-sec deposit with a particle size of about 2.6 nm]. Only a small portion of this loss can be attributed to the buildup of carbon on the surface, because such strong attenuation should not be produced by only a partial monolayer. The major part of this decrease in Ni signal is due to other changes in the particles induced by CO desorption, e.g., changes in morphology and/or dispersion.

For further investigation of gas-induced effects, several sample sets were prepared and subjected to various gas–thermal treatments. After these treatments, the particulate deposits were analyzed by TEM and compared with samples prepared under identical conditions and removed from the system "as deposited."

The first set of particulate deposits was grown with various Ni exposures and each sample was subjected to two CO desorptions. After these CO desorptions, the particle diameters were much larger than those of "as-deposited" samples with identical metal depositions. For a 25-sec deposit, nearly a 40% increase in diameter was observed, accompanied by only a small reduction of the particle number density. In combination with the AES results mentioned

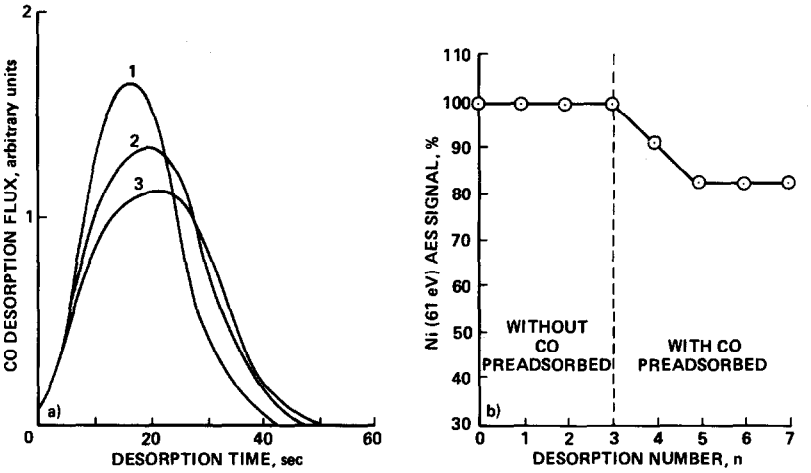

FIG. 9. The effect of CO adsorption–desorption cycles on the CO desorption peak position and the Ni 61-eV peak; (a) first three desorptions of a 25-sec Ni deposit, (b) Ni 61-eV Auger peak height before and after successive desorptions, first without adsorbed CO, then with adsorbed CO.

above (where a reduction in the Ni signal was observed with repeated CO desorptions), CO-induced coalescence of Ni particles below the detection limit of TEM could be responsible for this effect.

Next, three sets of five samples each were prepared. Samples within each set received the same metal exposure, but the deposition time was varied for the three sets—25, 50, and 200 sec, respectively. Each sample within a set received a different gas–thermal treatment: (1) no treatment (as deposited), (2) two CO desorptions, (3) a 10-min exposure to 5×10^{-7} Torr of O_2 at 300°C, (4) treatment 3 followed by a 10-min exposure to 5×10^{-7} Torr of H_2 at 300°C, and (5) a 6-L O_2 exposure followed by a 60-sec flash heating (maximum sample temperature of 200°C). TEM results of the above are shown in Fig. 10 (except treatment 5 which produced results similar to treatment 2).

As described earlier, treatment 2 (two CO desorptions) caused an increase in the diameter of the small particles. For the 25-sec deposits, treatments 2 and 5 also seem to produce particles with uneven contrast when seen in the TEM. The similarity of the two cases supports the idea that oxygen atoms from CO dissociation diffuse into the bulk of the particles. However, no evidence could be found by TED that bulk oxidation of Ni took place on any of the samples because of this treatment.

During the extended high-temperature oxygen exposure (treatment 3), particles oxidize and spread over the mica surface. For the shorter deposits (25 and 50 sec) and the small particles of the 200-sec deposit, complete oxidation of the Ni occurs and TED patterns show only epitaxially textured NiO. Right-angled particle habits frequently formed, which is consistent with the cubic lattice of NiO. The large particles of the 200-sec deposit do not totally oxidize and diffraction rings of both Ni and NiO are found. It is interesting to note, however, that the NiO shows some degree of preferred orientation, stemming from the epitaxial spreading of the oxide phase from the deposit.

Following the reduction treatment in hydrogen (treatment 4), much of the oxide produced by treatment 3 was converted back to Ni. In all deposits, the particles that are left after this final reduction are vastly altered from those of the "as-deposited" state. The average diameters of the particles in all deposits increased, and in the larger deposits (50 and 200 sec) fewer de-

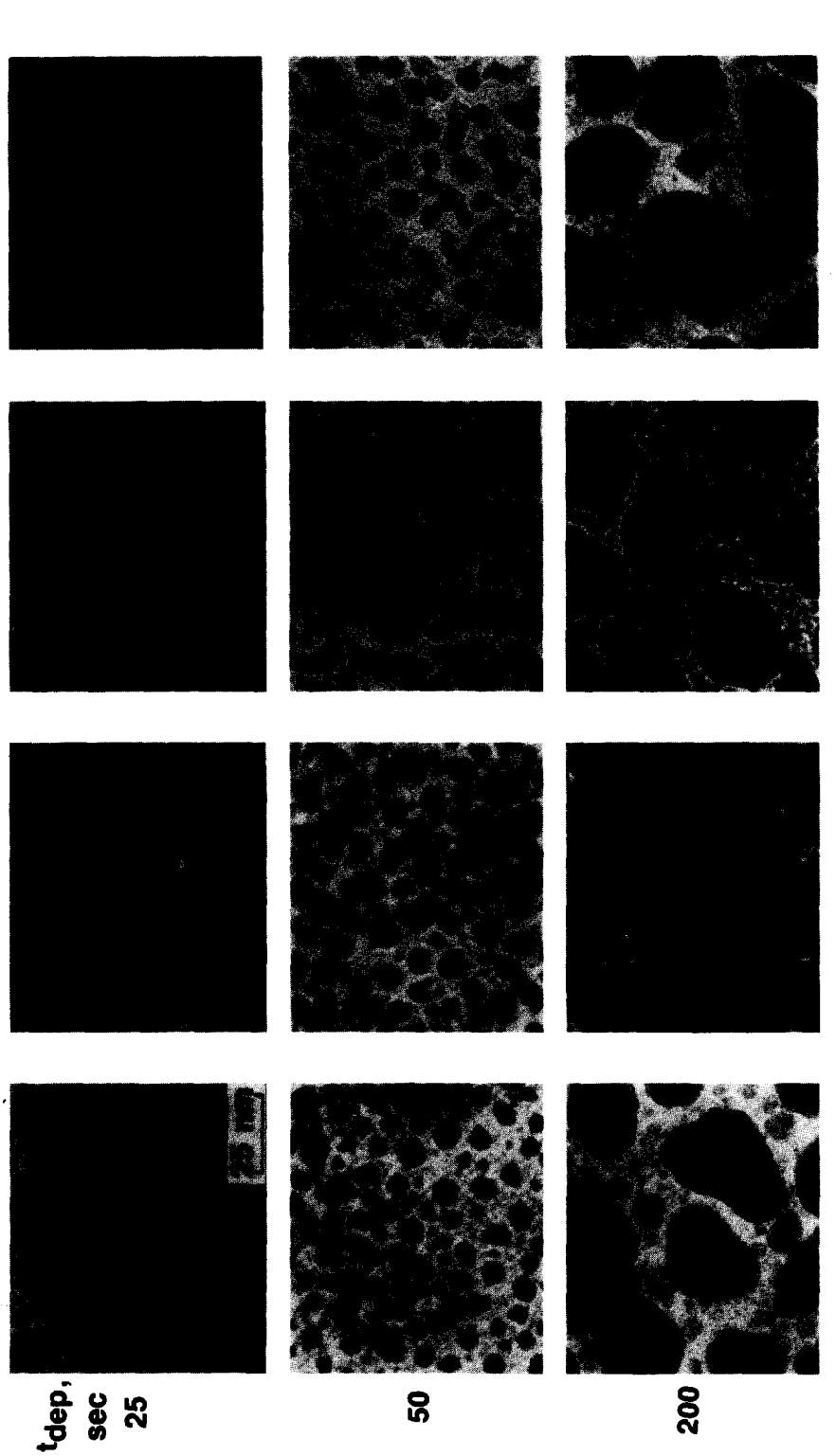

FIG. 10. The effect of gas–thermal treatments on the structure of Ni particles with deposition times of 25, 50, and 200 sec. TEM results for: (a) as deposited; (b) two CO desorptions (T_{max} = 200°C); (c) heat treated in oxygen (15 min, 300°C at 5×10^{-7} Torr); and (d) treatment c followed by heat treatment in hydrogen (15 min, 300°C at 5×10^{-7} Torr).

fects and twin boundaries were observed (as seen by the more uniform contrast within the particles). The small particles of the 200-sec deposit almost totally coalesced with the larger particles. However, the reduced particles still exhibit little or no increase in epitaxy compared to the "as-deposited" state.

DISCUSSION

CO has been well studied on single and polycrystalline Ni surfaces (*4–9*). On the low-index faces, CO is known to adsorb molecularly at room temperature, desorbing completely at around 160°C. Two other CO desorption peaks have also been produced at about 350°C (β_1) and 550°C (β_2) in a number of circumstances. These are due to the associative desorption of surface carbon and oxygen atoms. Madden and Ertl (*6*) were able to produce these states by heating the sample in a CO background to produce carbon on the surface and then dosing with oxygen prior to desorption. They found that if the carbon and oxygen coverages were increased, the β_1 peak was shifted in temperature to as low as 250°C, whereas the β_2 peak temperature was independent of the C and O coverage. From this they concluded that the β_1 peak was due to the recombination of mobile oxygen and carbon atoms on the Ni, and the β_2 peak was from oxygen combining with graphite nuclei. Erley and Wagner (*8*) were also able to reproduce these high-temperature desorption peaks with a stepped Ni (111) surface. In that case, the β_1 peak was interpreted as due to associative desorption from terrace sites, while the β_2 peak was due to desorption from step and kink sites. The decomposition was thus concluded to occur on surface defect structures during the desorption of molecularly adsorbed CO. They also suggested that CO binds to steps with a higher binding energy than on terraces as is the case for Pt (*20*), and CO decomposition takes place at a temperature below that for this site.

In our work, a number of similarities between small Ni particles and large stepped Ni single crystals have been observed. Small Ni particles grown on mica decompose CO at a rate that increases with diminishing particle size. This decomposition is at a temperature below where molecular desorption is completed. We assume that CO decomposes at specific surface sites, the density of which increases for smaller particle sizes.

One possibility is that CO dissociates on the edge and corner sites of the particles in a way similar to the step and kink sites on single-crystal Ni surfaces. Since their density increases with diminishing particle size (*21*), the higher CO decomposition activity of the smaller particles would be expected.

The metal–support interaction also increases with diminishing particle size. The higher number density of the Ni particles compared with that of other metals such as Pd (*16, 22*) or Au (*11*) grown under comparable conditions is evidence of the stronger interaction of Ni with mica. The fraction of Ni atoms that comes in contact with the mica surface also increases with diminishing particle size. This interaction could produce lattice distortions and/or changes in intrinsic electronic properties (*23–25*) of the particles that can lead to higher activity toward CO decomposition.

Since no associative desorption or reaction products were observed during the desorption, dissociated C and O atoms would be left on the sample. The C atoms remain bound to the surface as seen by AES and result in a continuous decay of the CO desorption peak with successive adsorption–desorption cycles. Oxygen atoms must either leave the surface (by reaction with CO to form CO_2, diffusion in the bulk of the particle, or incorporation into the mica substrate) or be immobile and prevented from reacting with the surface carbon. Since the carbon reacts easily with further oxygen adsorbed on the surface, the latter case is considered unlikely.

The β_1 peak of a C-contaminated sample dosed with O_2 was typically found around

250°C but decreased in temperature with oxygen dose. However, no shift in the peak was observed when only the carbon coverage was varied. Since both the carbon and the oxygen coverages were changed simultaneously in the experiment reported by Madden and Ertl (*6*), it is difficult to reach any conclusion about the reaction mechanisms from the desorption peak shift they observed. Our results imply that only the oxygen needs to be mobile on the particle surface.

The α desorption peak from the Ni particles also shifts in temperature with increasing preexposure to oxygen. This resulted in a dramatic reduction of the peak size with increasing O_2 exposure because of the lowered binding energy of the particle surface. (Equilibrium coverage of CO at the 50°C adsorption temperature was reduced by the low binding energy.) These results are again consistent with the work of Conrad *et al.* (*19*) on single-crystal Ni (111).

Physical changes of particles due to various gas–thermal treatments used in these studies were considerable. Although our results of these processes are very limited, it was, nevertheless, apparent that smaller Ni particles were affected more than large particles. These morphological changes included alterations in particle size and habit which were accompanied by changes in the CO binding energy. Perhaps the most surprising result was that these changes occurred at relatively low thermal and gas exposures when compared to similar results obtained with other transition metals during TEM studies at higher pressures and temperatures (*26, 27*). The possibility of such changes being readily produced during catalytic studies must therefore be seriously considered in future investigations of this nature.

CONCLUSIONS

The decomposition of CO occurs more readily on small Ni particles than on low-index faces of single crystals. This is similar to the interaction of CO with stepped Ni (111) bulk surfaces. The rate of CO decomposition is a strong function of particle size with the smallest particles exhibiting the fastest rate. This can lead to rapid contamination of the particle surface by carbon. It is probable that the oxygen atoms from CO decomposition do not remain on the surface because of several removal processes; oxygen could react with CO to form CO_2 as seen by Madden and Ertl (*6*) on Ni (111), or diffuse into the bulk of the Ni particles at elevated temperatures, or become incorporated into the mica lattice.

The associative desorption peak of C + O $\rightarrow$ CO is found on Ni particles only after dosing a contaminated sample with O_2 and the β_1 peak temperature was dependent on the oxygen coverage only. Changes in the carbon coverage only affected the area under the peak and not the peak temperature. Thus, it would appear that the recombination involves mobile oxygen and stationary carbon atoms. A β_1 peak is always accompanied by a reduction of the carbon Auger signal. Oxygen dosing of the Ni particles leaves residual oxygen on the particle surface which acts as a contaminant, blocking subsequent Co adsorption. This oxygen can be removed by heat treatment of the sample in H_2.

Some of the gas–thermal treatments frequently used in this study also altered the morphology and state of dispersion of the Ni particles. CO adsorption–desorption cycles caused gas-induced changes in particle size and shape, and a corresponding shift in the average CO binding energy. Coalescence and epitaxial ordering of NiO crystallites could be formed by extended O_2 exposures at elevated temperatures. H_2 reduction of the oxidized particles produced metal particles larger than the original "as-deposited" Ni particles and with fewer defects. All of these gas-induced effects were more complete on the smaller Ni particles, occurred at relatively low temperatures and gas pressures, and produced significant changes in the CO adsorption properties of the Ni particles. More system-

atic attention will have to be paid to particle morphology and dispersion in future model studies of supported metal particles under UHV conditions.

ACKNOWLEDGMENTS

This work was supported by NASA Contracts NCA2-OR840-801 and NCA2-OR840-002. The authors also wish to thank Dr. Rainer Anton for helpful discussions and access to unpublished results.

REFERENCES

1. McCarty, J. G., and Wise, H., *J. Catal.* **57,** 406 (1979).
2. Zagli, A. E., Falconer, J. L., and Keenan, C. A., *J. Catal.* **56,** 453 (1979).
3. Goodman, D. W., Kelley, R. D., Madey, T. E., and Yates, J. T., Jr., *J. Catal.* **63,** 226 (1980).
4. Christmann, K., Schober, O., and Ertl, G., *J. Chem. Phys.* **60,** 4719 (1974).
5. Tracy, J. C., *J. Chem. Phys.* **56,** 2736 (1972).
6. Madden, H. H., and Ertl, G., *Surf. Sci.* **35,** 211 (1973).
7. Joyner, R. W., and Roberts, M. W., *J. Chem. Soc. Faraday Trans. 1* **10,** 1819 (1974).
8. Erley, W., and Wagner, H., *Surf. Sci.* **74,** 333 (1978).
9. Eastman, D. E., Demuth, J. E., and Baker, J. M., *J. Vac. Sci. Technol.* **11,** 273 (1974).
10. Allpress, J. G., and Sanders, J. V., *Surf. Sci.* **7,** 1 (1967).
11. Elliot, A. G., *J. Vac. Sci. Technol.* **11,** 826 (1974).
12. Lee, E. H., Poppa, H., and Pound, G. M., *Thin Solid Films* **32,** 229 (1976).
13. Poppa, H., and Elliot, A. G., *Surf. Sci.* **24,** 149 (1971).
14. Lee, E. H., Ph.D. thesis, Stanford University, 1974.
15. Poppa, H., and Lee, E. H., *Thin Solid Films* **32,** 223 (1976).
16. Thomas, M., Dickinson, J. T., Poppa, H., and Pound, G. M., *J. Vac. Sci. Technol.* **15,** 568 (1978).
17. Redhead, P. A., *Vacuum* **12,** 203 (1962).
18. Doering, D. L., Poppa, H., and Dickinson, J. T., *J. Vac. Sci. Technol.* **17,** 198 (1980).
19. Conrad, H., Ertl, G., Kuppers, J., and Latta, E. E., *Surf. Sci.* **57,** 475 (1976).
20. Collins, D. M., and Spicer, W. E., *Surf. Sci.* **69,** 85 (1978).
21. Van Hardeveld, R., and Hartog, F., *Surf. Sci.* **15,** 189 (1969).
22. Doering, D. L., Poppa, H., and Dickinson, J. T., *J. Catal.* **73,** 104 (1982).
23. Hamilton, J. F., and Baetzold, R. C., *Science* **205,** 1213 (1979).
24. Anderson, J. R., Foger, K., and Breakspere, R. J., *J. Catal.* **57,** 458 (1979).
25. Vannice, M. A., and Garten, R. L., *J. Catal.* **56,** 236 (1979).
26. Anton, R., Heinemann, K., and Poppa, H., *in* "Proceedings, International Vacuum Congress" (F. Abeles and M. Croset, Eds.), pp. 121. Paris, France, 1980.
27. Chen, M., and Schmidt, L. D., *J. Catal.* **56,** 198 (1979).